Exploration of the high temperature phase evolution of electrochemically modified $Sc_2(WO_4)_3$ via potassium discharge

Received 00th January 20xx,
Accepted 00th January 20xx

DOI: 10.1039/x0xx00000x

Junnan Liu,[a] Abby R. Haworth,[b] Karen E. Johnston[b], Damian Goonetilleke,[a] and Neeraj Sharma[a*]

The electrochemical modification of $Sc_2(WO_4)_3$ via activation as an electrode against potassium metal is investigated, as well as the subsequent thermal evolution of activated $Sc_2(WO_4)_3$. Upon discharge to 0.01 V versus K/K^+, $Sc_2(WO_4)_3$ delivers a capacity of 132 mAh g^{-1}. On subsequent heating from 100 to 623 K the discharged electrode exhibits essentially the same thermal expansion as that of the pure powder. Between 673 and 973 K a trigonal K_2WO_4-type phase (*P*-3*m*1) is formed. Variable-temperature X-ray diffraction data indicates that upon heating from 923 K - 1023 K, this phase has a thermal expansion coefficient of -1.90(10) x 10^{-4} K^{-1}.

Introduction

Negative thermal expansion (NTE) materials exhibit a net contraction in their volume upon heating. NTE has been observed in a variety of different materials, including metal organic frameworks (MOFs),[1-3] polymers,[4] magnetic alloys,[5] and ceramics.[6, 7] The structural mechanism by which NTE is achieved in these materials appears to be unique to each. For example ZrW_2O_8 has generated considerable interest as it exhibits isotropic NTE over a large temperature range (0.3 – 1050 K).[8, 9] Further various molybdates and tungstates of the type $A_2(MO_4)_3$, where A is cation coordinated octahedrally to oxygen and M = Mo, W, V tetrahedrally coordinated to oxygen, have been shown to exhibit interesting thermal expansion behaviour.[9-12] The structure of $A_2(MO_4)_3$ contains large voids which allow for the correlated movement of the MO_4 tetrahedral and AO_6 octahedral units to form a more compact unit cell upon heating.[10, 13] One such material is $Sc_2(WO_4)_3$, whose structural evolution as a function of temperature has been studied in detail by Evans *et al*.[14] $Sc_2(WO_4)_3$ adopts an orthorhombic structure with space group *Pnca* from 10 - 450 K, over which a volumetric thermal expansion coefficient of $\alpha_V = -6.5 \times 10^{-6}$ K^{-1} is observed.[14]

The large spatial voids present in NTE materials such as $A_2(MO_4)_3$ makes them ideal insertion materials, where a guest species or ion can be reversibly inserted and removed, ideally, without significant degradation of the structure.[15] Such materials could act as suitable hosts for alkali ions such as lithium, sodium or potassium and, hence, function as electrode materials in alkali-ion batteries.[16] Furthermore, the controlled electrochemical insertion of these alkali ions could result in materials with modified or enhanced physical properties. The use of electrochemistry (and/or thermal treatments) to synthesise or modify materials has been successfully demonstrated, allowing for fine control of the quantity of guest ions inserted, thereby enabling phases with very specific compositions (which may otherwise be difficult to synthesise) to be explored.[17, 18]

The use of electrochemical activation to modify the properties of a material has previously been investigated for systems in the $A_2(MO_4)_3$ series, such as $Sc_2(WO_4)_3$, $Al_2(WO_4)_3$ and $Sc_2(MoO_4)_3$.[16, 19] After electrochemical modification via the insertion of sodium into the structure, the $Sc_2(WO_3)_4$ structure was found to be retained upon heating up to 698 K. Heating beyond this temperature resulted in different phase evolution depending on the "extent" of electrochemical discharge, i.e., the amount of Na inserted into the electrode. The "extent" is characterised by the amount of capacity delivered by the electrode, with 100 % discharge considered to be maximum capacity. The 50 % sodium discharged $Sc_2(WO_3)_4$ decomposed upon heating to form amorphous or nanocrystalline phases, whilst the 75 % discharged $Sc_2(WO_3)_4$ formed new phases that were tentatively assigned as Sc_6WO_{12} and additional unknown phases.[19] The 12.5 % and 25 % lithium discharged samples were found to transition to a $Sc_{0.67}WO_4$-type phase at ≈ 900 K, the synthesis of which had only previously been reported at temperatures and pressures of at least 1673 K and 4 GPa.[20] Similar studies involving the electrochemical modification of the $Ta_xV_{1-x}O_5$ system using sodium, lithium, and potassium were found to result in interesting phase evolution as a function of temperature, including the generation of new phases.[21] In particular, for the 25 % sodium discharged $TaVO_5$, the volumetric thermal expansion coefficient of the $TaVO_5$-like phase produced increased significantly, to $\alpha_V = -5.75 \pm 0.20 \times 10^{-5}$ K^{-1}.

In this study, the electrochemical storage capability of $Sc_2(WO_4)_3$ as a host electrode for potassium ions is presented. Solid-state nuclear magnetic resonance (NMR) is used to investigate the local environment of the inserted K in the 100 % potassium discharged sample. Variable-temperature synchrotron X-ray diffraction data is obtained for discharged variants of $Sc_2(WO_4)_3$ to determine the influence of electrochemical modification on the phase evolution of $Sc_2(WO_4)_3$. The thermal treatments clearly show the formation of new phases, similar to previous work on Li and Na electrochemically activated $Sc_2(WO_4)_3$.[19, 20] However, in contrast to these studies, K-based electrochemical activation forms at least one phase conventionally synthesised via other routes. A α-K_2WO_4 phase, which adopts space group *P*-3*m*1, is observed after heating the K discharged $Sc_2(WO_4)_3$ electrode to 623 K. This phase was found to exhibit an NTE coefficient of $\alpha_V = -1.9(1) \times 10^{-4}$ K^{-1} during heating from 923 K to 1023 K. The

[a] *School of Chemistry, UNSW Sydney, Sydney NSW 2052, Australia*
[b] *Department of Chemistry, Durham University, South Road, Durham DH1 3LE, United Kingdom*
Corresponding author: N. Sharma, neeraj.sharma@unsw.edu.au
† Footnotes relating to the title and/or authors should appear here.
Electronic Supplementary Information (ESI) available: [details of any supplementary information available should be included here]. See DOI: 10.1039/x0xx00000x

structure of α-K_2WO_4 has not previously been refined in the *P*-3*m*1 space group, and the observed volumetric expansion coefficient is among the largest to be reported.[22]

Experimental

Sample Preparation

The synthesis and structural characterisation of $Sc_2(WO_4)_3$ has been detailed previously.[14] Polycrystalline $Sc_2(WO_4)_3$ was prepared using the constituent oxides via conventional solid-state synthesis. Stoichiometric quantities of Sc_2O_3 (Sigma Aldrich, 99.9 %) and WO_3 (Carlo Erba, 99 %) were thoroughly mixed, ground in an agate mortar and pestle and heated (at 6 °C min^{-1}) in an alumina crucible to 1000 °C, held for 12 hours, and cooled to room temperature. The sample was then ground and heated to 1200 °C for another 12 hours.

Electrode Preparation

Electrodes were prepared by casting a slurry consisting of a mixture of 80 % active material ($Sc_2(WO_4)_3$), 10 % carbon black (Timcal C65) and 10 % polyvinylidene difluoride (PVDF, MTI Corporation) dissolved in n-methyl-2-pyrrolidone (NMP) solvent. The slurry was stirred overnight before being cast as a 200 µm thick layer on a Cu foil substrate. The cast electrode was dried in a vacuum oven at 100 °C overnight, followed by pressing at 100 kN for one hour in a hydraulic press. The electrode was returned to the vacuum oven for two hours before being transferred to an Ar-filled glovebox for coin cell construction. In the glovebox, 16 mm diameter electrodes were punched and used in the construction of potassium half-cells.

Electrochemistry

All electrodes were cycled against K metal with 1 M KPF_6 in a 50:50 ethylene carbonate (EC) and dimethyl carbonate (DMC) solution used as the electrolyte. Cells were constructed in an Ar-filled glovebox by assembling the electrode, electrolyte-soaked glass-fibre separator and K metal in a CR2032 coin cell. The cells were allowed to rest for 24 hours before cycling. Electrochemical discharge curves were recorded using a Neware Battery Testing System under galvanostatic conditions, where cells were discharged to 0.01 V and charged to 2.5 V at 10 mA g^{-1}. For *ex situ* studies of the potassium inserted electrode material, cells were discharged to 0.01 V, which is 100 % of the total capacity versus K at 10 mA g^{-1}. Upon reaching the desired state of discharge, the coin cells were immediately transferred to the glovebox, where the electrode was extracted to minimize any relaxation phenomena, washed with DMC and left to dry overnight. The dried electrode materials were packed in 0.5 mm diameter quartz capillaries and sealed under Ar for variable-temperature XRD studies or packed into Kel-F inserts for NMR analysis.

Solid-State NMR Spectroscopy

Solid-state NMR spectra were acquired using either a Varian VNMRS or Bruker Avance III HD spectrometer, equipped with a wide-bore 9.4 T or 11.7 T magnet using Larmor frequencies of 18.67 MHz and 121.49 MHz for ^{39}K and ^{45}Sc, respectively. Inside an Ar-filled glovebox, samples were packed into inserts, placed into 4 mm ZrO_2 rotors and spun at magic-angle spinning (MAS) rates of 8 and 10 kHz. ^{39}K chemical shifts were referenced to 1 M $KCl_{(aq)}$ and ^{45}Sc chemical shifts were referenced to 0.06 M $Sc(NO_3)_3$ in D_2O using the proton signal of neat tetramethyl silane (TMS) and the frequency ratio. ^{39}K MAS NMR spectra were acquired using a spin echo experiment (90_x-τ-180_y) with optimized pulse lengths of 8.6 and 16.6 µs and a recycle delay of 1 s. Conventional ^{45}Sc MAS NMR spectra were obtained using a single pulse experiment with an optimized pulse length of 2.5 µs and a recycle delay of 0.4 s.

X-ray diffraction

Variable-temperature (VT) X-ray diffraction (XRD) experiments were undertaken using laboratory and synchrotron XRD. Variable temperature experiments from 100 K to 450 K were undertaken on a Bruker D8 Advance diffractometer, using an Oxford Cryostream and Mo Kα radiation, with a ramp rate of 20 K per hour. Diffraction data were collected every 30 mins. High temperature evolution was studied using high resolution synchrotron XRD between 323 – 1023 K. High temperature experiments were undertaken using a FMB Oxford hot-air blower on the Powder Diffraction Beamline at the Australian Synchrotron using a wavelength of λ = 0.68885(1) Å, determined using a LaB_6 660b standard reference material (SRM).[23] The data were collected in 50 K intervals from 298 K to 673 K and then in 25 K intervals until 1023 K. Upon cooling to room temperature, data were also collected at 623 K, 423 K and 298 K. Rietveld analysis were performed with structural models and diffraction data using GSAS-II.[24] The refinements were carried out based on $Sc_2(WO_4)_3$ adopting orthorhombic *Pnca* space group symmetry and trigonal *P*-3*m*1 and *Ccmm* space group symmetries of K_2WO_4. Crystal structure illustrations were rendered using VESTA.[25]

Elemental composition

Inductively coupled plasma optical emission spectroscopy (ICP-OES) was undertaken to confirm the elemental composition in the as-prepared and discharged samples. The samples were dissolved in aqua regia before measurement on a Perkin Elmer Optima7300DV.

Results and discussion

Electrochemical performance of $Sc_2(WO_4)_3$

$Sc_2(WO_4)_3$ electrodes were discharged to a cut-off potential of 0.01 V. The corresponding discharge profile is shown in Figure 1(a). At the end of discharge, 4.1 K^+ ions per formula unit were inserted into the $Sc_2(WO_4)_3$ structure, corresponding to a capacity of 132 mAh g^{-1}. The voltage profile displays a smooth decrease in potential with no distinct plateaus observed, suggesting either solid-solution[26] or surface-based reactions taking place. Longer term cycling of $Sc_2(WO_4)_3$ electrodes was also investigated. However, the capacity retention was unfavourable, reducing to ~10 mAh g^{-1} by the 20th cycle (Figures 1(a) and (b)). XRD data was collected for the extracted electrode at the end of the 1st discharge and is shown in Figure 2a (and this is referred to as 100 % K discharge). Rietveld refinement of the structural models with the XRD data confirms that the $Sc_2(WO_4)_3$ structure is retained after the 1st discharge, albeit with minor changes in lattice parameters relative to the pristine $Sc_2(WO_4)_3$ electrode. A comparison of the lattice parameters for the pristine and discharged samples is given in Table 1.

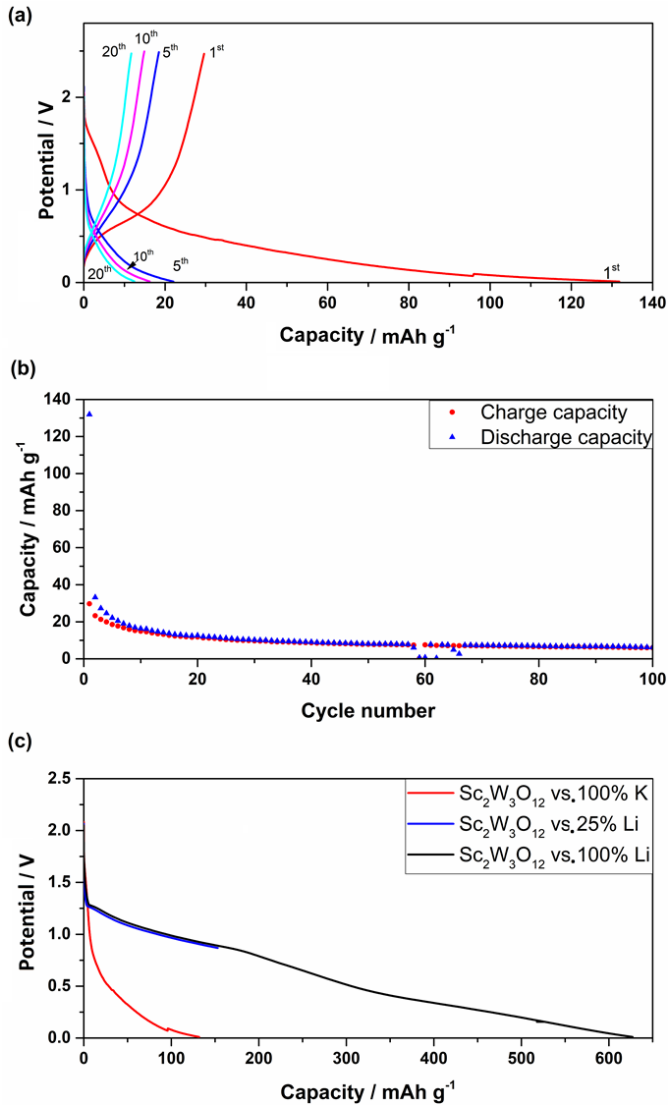

Figure 2(a) Potential profiles of $Sc_2(WO_4)_3$ electrodes versus K at different cycle numbers. (b) Capacity retention as a function of cycle number at 10 mA g^{-1}. (c) Comparison of $Sc_2(WO_4)_3$ electrodes discharged to 100 % capacity in K half cells, and 25 % and 100 % capacity in Li half cells.

$Sc_2(WO_4)_3$ delivers a capacity of 132 mAh g^{-1} upon discharge to 0.01 V versus potassium, which is in between the capacities previously reported in studies of lithium discharged samples,[20, 27] where capacities of 83.5 mAh g^{-1} and 167 mAh g^{-1} were observed for the 12.5 % and 25 % lithium discharged electrodes respectively. It is noted that, in both lithium discharge cases, the pristine phase was retained at these levels of discharge. However, the electrodes were shown to undergo phase transitions after thermal treatment.[19, 20] A Fourier difference map of potassium discharged $Sc_2(MoO_4)_3$ was generated, see Figure 2b, which shows small regions of electron density in the parent structure which may indicate a small amount of intercalation into the structure. ICP-OES results indicate 1.41 weight% of K in the discharged sample.

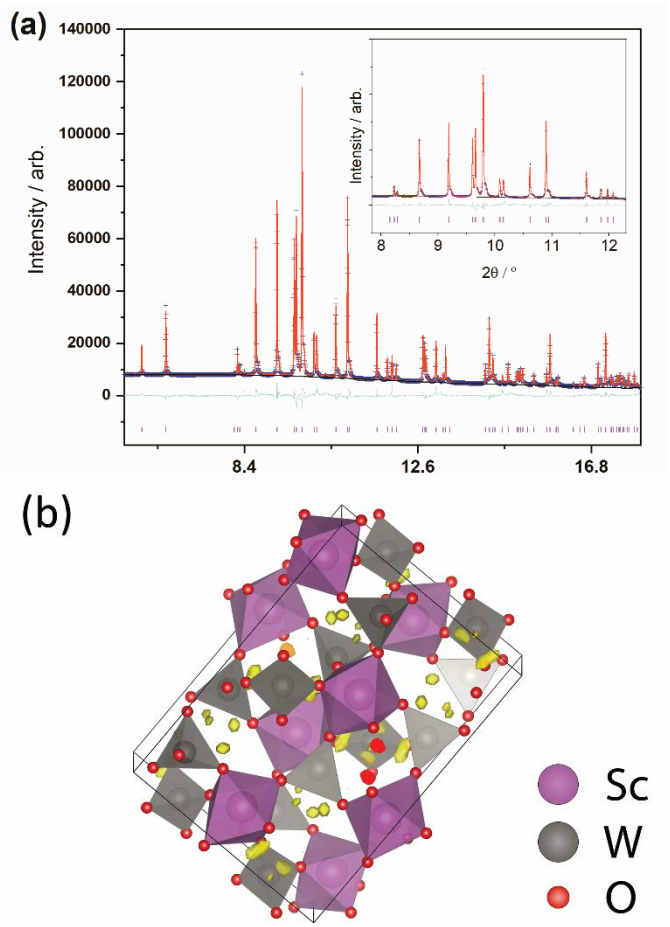

Figure 1 a) Rietveld refinement of the $Sc_2(WO_4)_3$ structural model with XRD data obtained from a $Sc_2(WO_4)_3$ electrode extracted after discharge to 100 % in K half cells (R_{wp} = 7.816 %). The data was refined using the *Pnca* model. An expansion of the region 2θ = 8 – 12° is also shown as an inset. The data are shown in blue, the calculated model is in red, the difference between the data and model is shown in cyan and the magenta markers are the Bragg reflections for $Sc_2(WO_4)_3$. b) Fourier difference map of potassium discharged $Sc_2(MoO_4)_3$ where the the yellow regions are the electron density.

Table 1 Refined lattice parameters for pristine $Sc_2(WO_4)_3$ and 100 % K discharged $Sc_2(WO_4)_3$, obtained from the Rietveld analysis shown in Figure 2.

	a (Å)	*b (Å)*	*c (Å)*
$Sc_2(WO_4)_3$	9.6735(2)	13.3218(3)	9.5812(2)
100 % K discharged $Sc_2(WO_4)_3$	9.6715(1)	13.3193(2)	9.5792(1)

Solid-State NMR Studies of K discharged $Sc_2(WO_4)_3$

To assist in understanding the structural changes occurring upon discharge, ^{45}Sc and ^{39}K MAS NMR studies were undertaken for the 100 % potassium discharged $Sc_2(WO_4)_3$ electrode and are shown in Figure 3. The ^{45}Sc MAS NMR spectrum (Figure 3(a)), exhibits a single resonance at δ = 14.5 ppm, in good agreement with the *Pnca* crystal structure, a single crystallographic site. A spectrum with wide spectral width was also acquired and fitted to obtain the corresponding quadrupolar parameters. The single site has a quadrupolar coupling constant, C_Q = 2.3(1) MHz, and an asymmetry parameter, η_Q = 0.5 (1). Based on the parameters obtained and, in particular the relatively low value of C_Q, the Sc environment appears to be highly symmetrical, in good agreement with the reported crystal structure and the presence of a symmetrical 6-coordinate Sc site. However, it is noted that the chemical shift observed is not consistent with that of a 6-coordinate environment, which typically exhibits a much higher chemical shift, closer to $\delta \approx 150$ ppm.[28] The substantial difference in chemical shift observed here is indicating something very specific about the local structural environment. More specifically, given the nature of the system under investigation, it is likely that the observed chemical shift is providing information regarding the location of the inserted K^+ ions. The shift observed suggests a proportion of the K^+ ions are located close to the ScO_6 sites in the $Sc_2(WO_4)_3$ structure or near the surface. At present, there are still relatively few publications detailing the chemical shift ranges observed for ^{45}Sc. Hence, we can only postulate as to what may be causing these changes. Based on the severity of the change, it is highly likely that the position of K or the nature of K in the crystal structure or its surrounds is influencing the local Sc environment and therefore the chemical shift. To gain additional insight into the K local environment, ^{39}K solid-state NMR studies were also explored.

With a natural abundance of 93.3 %, ^{39}K appears to be a suitable nucleus for study by solid-state NMR. However, it is a low-γ nuclide with a small magnetic moment and unfavourable quadrupolar characteristics, meaning the number of ^{39}K solid-state NMR studies are still relatively limited. Furthermore, based on its unfavourable characteristics, specialist hardware is required to acquire ^{39}K MAS NMR spectra, namely a low-γ tuning accessory. The ^{39}K MAS NMR spectrum obtained for the 100 % potassium discharged $Sc_2(WO_4)_3$ electrode is shown in Figure 3(b) and exhibits a single, very narrow resonance at δ = −39.0 ppm. Based on the spectrum obtained, the quadrupolar coupling constant is too small to measure (*i.e.*, the lineshape is too narrow and featureless to obtain a meaningful and truly representative value). The presence of a very sharp resonance suggests potassium from the discharge step is located in a highly symmetrical environment. As stated earlier, the *Pnca* structure of $Sc_2(WO_4)_3$ contains numerous large voids, all of which are potential host sites for the inserted K ions. The ^{39}K MAS NMR spectrum provides evidence that the K local environment highly symmetrical which may indicate a proportion of K has been inserted into the $Sc_2(WO_4)_3$ structure. It is interesting to note the well-defined nature of the K local environment rather than a distribution of environments. Given the limited number of ^{39}K NMR studies completed to date, very little chemical shift information is currently available within the literature. Hence, it is not possible to comment on the observed ^{39}K chemical shift and its precise structural meaning. However, it is noted that the chemical shift observed is within the range reported in other ^{39}K NMR studies.[29] The fact that the inserted K species can be probed is extremely encouraging for the exploration of other K discharged samples.

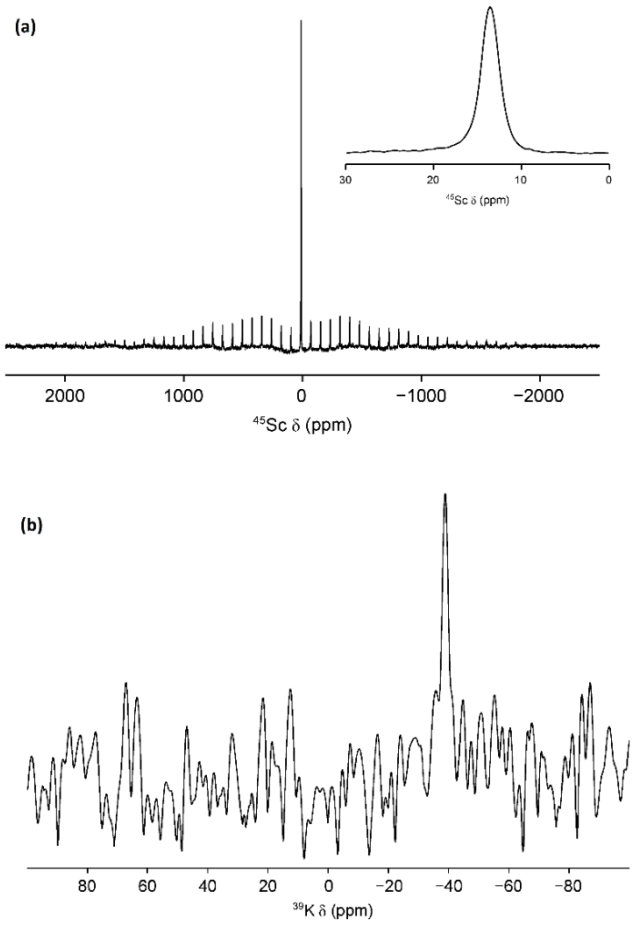

Figure 3 Conventional solid-state (a) ^{45}Sc and (b) ^{39}K MAS NMR spectra obtained for 100 % K discharged $Sc_2(WO_4)_3$. In (a) a spectrum with wide spectral width is shown. An expansion of the central-transition is also shown as an inset. MAS rates of (a) 10 kHz and (b) 8 kHz were used.

Variable-Temperature XRD Studies

To determine the influence of potassium discharge on $Sc_2(WO_4)_3$ phase evolution, variable-temperature *ex situ* XRD studies were completed for an extracted discharged $Sc_2(WO_4)_3$ (1st discharge) over the temperature range 100 - 1023 K in separate sub-ambient and high temperature experiments.

For sub-ambient experiments, the sample was first cooled to 100 K, heated to 450 K and then cooled back to 100 K. The corresponding variable-temperature XRD data is presented as a 2D contour map in Figure 4(a) and selected Rietveld-refined fits of the data at various temperatures are shown in Figure 4(b). The evolution of the lattice parameters as a function of temperature are shown in Figure 4(c). In this regime, the potassium discharged $Sc_2(WO_4)_3$ phase exhibits a rate of change in cell volume of $-7.19(1) \times 10^{-3}$ Å^3 K^{-1} during heating and $7.55(1) \times 10^{-3}$ Å^3 K^{-1} during cooling, compared to -8×10^{-3} Å^3 K^{-1} reported for pure $Sc_2(WO_4)_3$ during heating.[14] This corresponds to an overall volumetric expansion coefficient $\alpha_V = -5.79(1) \times 10^{-6}$ K^{-1} during heating and $\alpha_V = -6.1(1) \times 10^{-6}$ K^{-1} during cooling. The overall contraction of the structure during heating corresponds to a decrease in the *a* and *c* axes and an increase in the *b* axis, whilst the opposite trend is observed on cooling. The expansion coefficients for each axis (on heating and cooling) are given in Table 2. When compared to the pristine $Sc_2(WO_3)_4$ powder and electrode, this suggests that the K discharged $Sc_2(WO_4)_3$ electrode does not significantly alter the low temperature NTE properties.

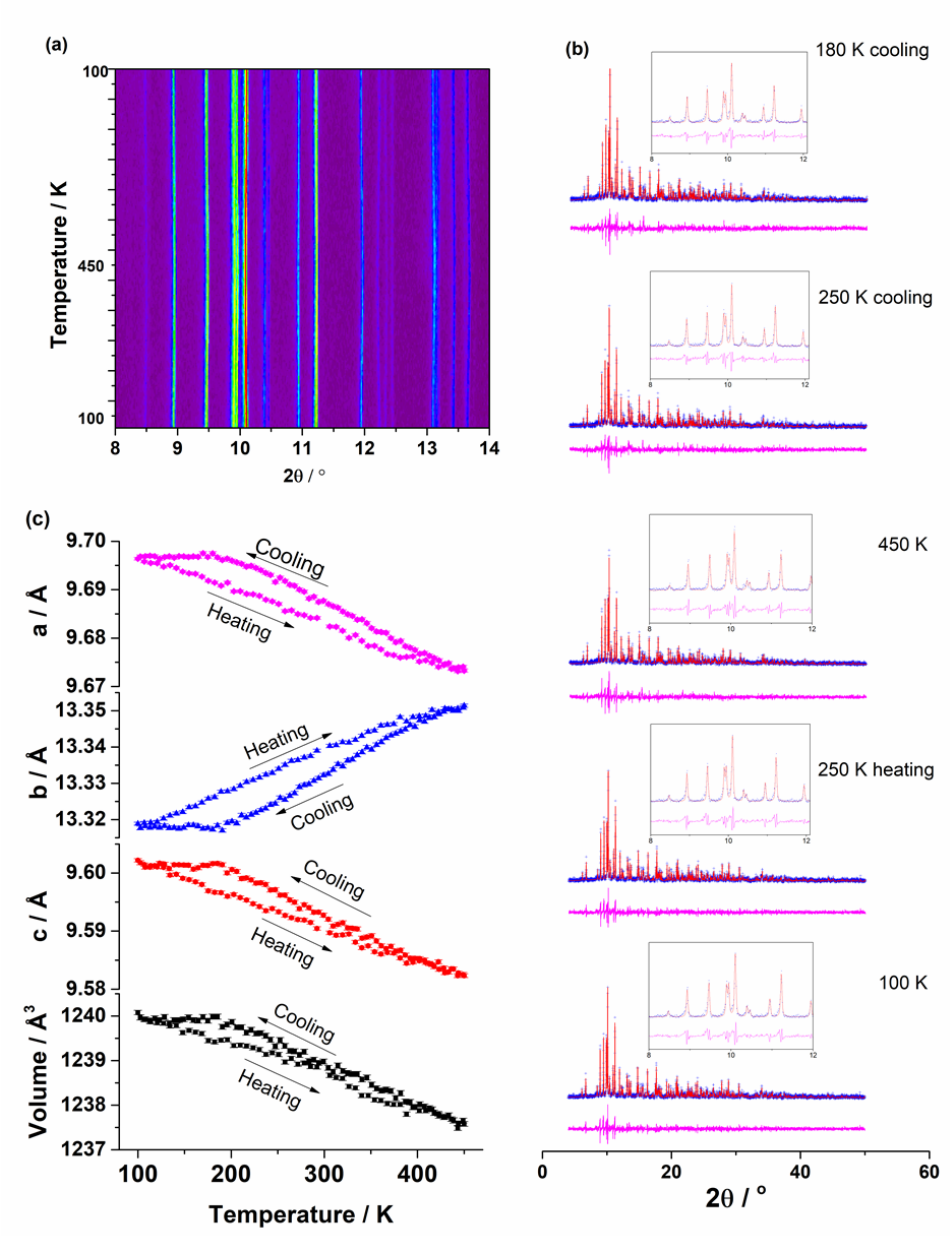

Figure 4(a) Variable-temperature XRD data obtained for the 100 % discharged $Sc_2(WO_4)_3$ electrode (in EC/DMC electrolyte after extraction), (b) selected Rietveld-refined fits obtained at different temperatures and (c) the corresponding variation in the lattice parameters and cell volume as a function of temperature.

Table 2 Axial (α_a, α_b, α_c) and volumetric (α_v) thermal expansion coefficients of a pristine $Sc_2(WO_4)_3$ and K discharged $Sc_2(WO_4)_3$ electrode estimated from lattice parameters determined using Rietveld analysis.

Sample	$\alpha_a \times 10^{-6}$ K^{-1}	$\alpha_b \times 10^{-6}$ K^{-1}	$\alpha_c \times 10^{-6}$ K^{-1}	$\alpha_{vol} \times 10^{-6}$ K^{-1}
$Sc_2(WO_4)_3$ K discharged (100-450 K, heating)	-7.39(2)	8.26(2)	-5.99(1)	-7.19(1)
$Sc_2(WO_4)_3$ K discharged (450-100 K, cooling)	7.92(3)	-8.39(2)	6.61(2)	7.55(1)
$Sc_2(WO_4)_3$ electrode (298-623 K)	-8.0(5)	4.4(4)	-5.3(4)	-0.87(5)
$Sc_2(WO_4)_3$ K discharged (298-623 K)	-10.9(1)	4.4(5)	-8.3(10)	-1.5(3)

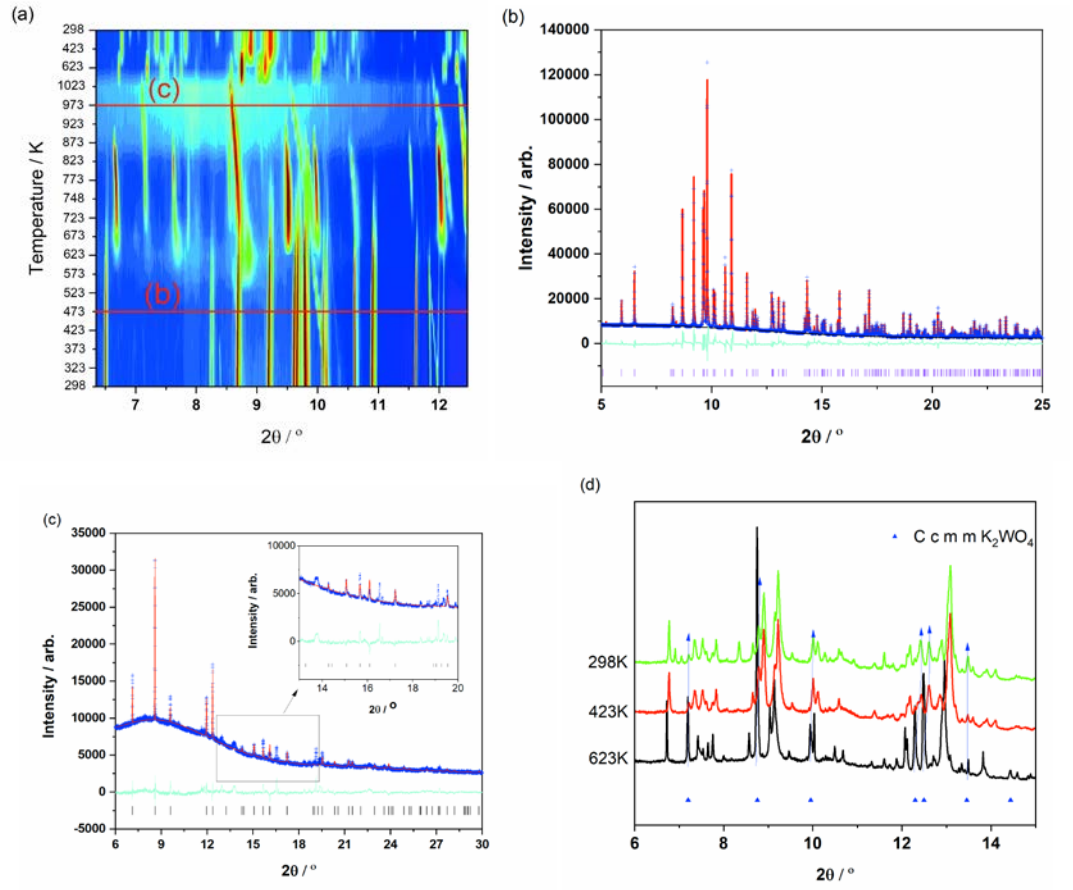

Figure 5 (a) Variable-temperature XRD data showing the thermal evolution of 100 % discharged $Sc_2(WO_4)_3$ electrode in EC/DMC containing electrolyte after extraction. Rietveld refinements of structural models with data obtained at (b) 473 K and (c) 973 K using (b) the *Pnca* model of $Sc_2(WO_4)_3$, R_w = 7.8 %, and (c) the *P*-3*m*1 K_2WO_4 model, R_w = 3.76 %. (d) XRD data on cooling to room temperature with peak markers for the *Ccmm* phase of K_2WO_4 indicated. In (b) and (c) the data are shown in blue, the calculated model is in red, the difference between the data and model is shown in cyan and the magenta and black markers are the allowed reflections for the $Sc_2(WO_4)_3$ and K_2WO_4 phases, respectively.

The variable-temperature *ex situ* XRD data obtained for K discharged $Sc_2(WO_4)_3$ from room temperature up to 1023 K and back to room temperature, is presented as a 2D contour map in Figure 5(a) with Rietveld-refined fits of structural models with XRD data at 473 K and 973 K shown in Figure 5(b) and (c), respectively. From room temperature up to 623 K, the $Sc_2(WO_4)_3$ structure is retained, as demonstrated in Figure 6, where the change in lattice parameters is characteristic of the NTE behaviour exhibited by the parent $Sc_2(WO_4)_3$ (also shown in Figure 6 for comparison). The rate of change in the cell volume for the $Sc_2(WO_4)_3$ electrode between 298 – 623 K was found to be -1.83(3) × 10^{-2} Å^3 K^{-1} larger than the literature values of -8 × 10^{-3} Å^3 K^{-1} for the pristine $Sc_2(WO_4)_3$ material, *i.e.*, not as an electrode.[14] However, it is noted that the data presented here is over a greater temperature range when compared to that in the literature (0 - 500 K). The coefficients for the $Sc_2(WO_4)_3$ electrode and the 100 % K discharged $Sc_2(WO_4)_3$ between 298 and 623 K are also shown in Table 2. Both the $Sc_2(WO_4)_3$ electrode (or 0 % discharged) and the 100 % K discharged $Sc_2(WO_4)_3$ electrode have a larger volume contraction when compared to pristine $Sc_2(WO_4)_3$. This implies that the PVDF and carbon black are slightly influencing the NTE behaviour of the electrode. The potassium discharged $Sc_2(WO_4)_3$ has larger NTE coefficients along the *a* and *c* axes which lead to the larger coefficient of volumetric expansion compared with non-discharged 0 % $Sc_2(WO_4)_3$ electrode up to 623 K.

Table 3: Comparison of the bond lengths (Å) of the refined K_2WO_4 phase and the K_2SO_4 phase used as the initial model.

K_2WO_4		K_2SO_4	
Bond	Length (Å)	Bond	Length (Å)
K(1) - O(2)	2.803(1)	K(1) - O(2)	2.520
K(2) - O(2)	2.619(3)	K(2) - O(2)	3.075
K(3) - O(1)	2.800(2)	K(3) - O(2)	2.933
W - O(1)	1.921(2)	S - O(1)	1.490
W - O(2)	1.914(2)	S - O(2)	1.430

The 100 % K discharged electrode shows substantial structural changes as the temperature is increased, in contrast to the pristine $Sc_2(WO_4)_3$ and $Sc_2(WO_4)_3$ electrode. Note $Sc_2(WO_4)_3$ has been reported to be stable up to 1023 K.[30] For 100 % K discharged $Sc_2(WO_4)_3$ between 673 and 873 K, new reflections appear, indicating the formation of additional phases (Figure 5(a)). The appearance of these new phases appears to coincide with the temperature at which PVDF decomposes.[19] Although some of the reflections could not be indexed, Rietveld analysis using α-K_2SO_4 as the structural model, in space group *P*-3*m*1,[31] was found to fit the 973 K XRD data (Figure 5(c)). Note that this model had initial lattice parameters of *a* = 5.71 Å and *c* = 7.85 Å. Replacing S^{6+} (r(S^{6+} ionic radii) = 0.29 Å) with W^{6+} (r(W^{6+} ionic radii) = 0.6 Å), an increase in lattice parameters is observed, as expected (Table 3). For Rietveld analysis, the bond lengths of the W-O and K-O in the α-K_2SO_4 model were constrained to 1.89 Å and 2.795 Å, respectively.[32] The subsequent fit is shown in Figure 5(c) and the crystallographic details are presented in Table 4. Note, this *P*-3*m*1 phase has previously been reported to be stable at 760 K. However, very few structural details were provided.[31] In the XRD data presented, K_2WO_4, in space group *P*-3*m*1 initially forms around 623 K and increases in concentration until 923 K after which it is the major phase. Above 923 K only minor impurity reflections are observed at 2θ ~ 13.76 °, 16.55 ° and 19.12 °. The change in lattice parameters between 923 and 1023 K are shown in Table 5. This change corresponds to a thermal expansion coefficient of α_V = -1.90(10) x 10^{-4} K^{-1} for K_2WO_4. The data presented suggests that K_2WO_4 produced via the thermal evolution of K discharged $Sc_2(WO_4)_3$ electrodes exhibits NTE behaviour between 923 and 1023 K. The thermal expansion is anisotropic with expansion along the *c* axis and contraction along the *a* axis. The coefficient of thermal expansion is α_c = 4.894(1) × 10^{-5} K^{-1} along the *c* axis and α_a = -1.225(1) × 10^{-4} K^{-1} along the *a* axis.

To date, the highest NTE coefficients reported for ceramics are the charge transfer material $Bi_{0.95}La_{0.05}NiO_3$ which has a volumetric expansion coefficient of α_V = -4.13 x 10^{-8} K^{-1} between 300 and 370 K,[33] the reduced layered ruthenate Ca_2RuO_4, α_V = -1.15 x 10^{-8} K^{-1} from 135 K to 345 K,[34] and the anti-perovskite $Mn_3Zn_{0.9}Ge_{0.1}N$ which has a coefficient of -2.28 x 10^{-4} K^{-1} between 202 and 222 K [35]. The NTE coefficients above were observed at lower temperature ranges compared to K_2WO_4 reported here which exhibits NTE behaviour between 923 K and 1023 K. This is the largest negative thermal expansion coefficient observed to date within this high temperature range.

Despite our observations, some studies suggest that K_2WO_4 adopts a hexagonal structure above 733 K. For example, studies have suggested a pseudo-hexagonal structure between 683 - 733 K, transitioning to an orthorhombic structure between 643 - 683 K and finally adopting monoclinic symmetry *C*2/*m* below 643 K.[36, 37] Structural transitions in this system are typically associated with reorientation of the WO_4^{2-} tetrahedra.[38] Some studies have suggested hysteresis of the phase transitions, depending on whether the sample is being heated or cooled, *i.e.*, the onset temperature for the phase

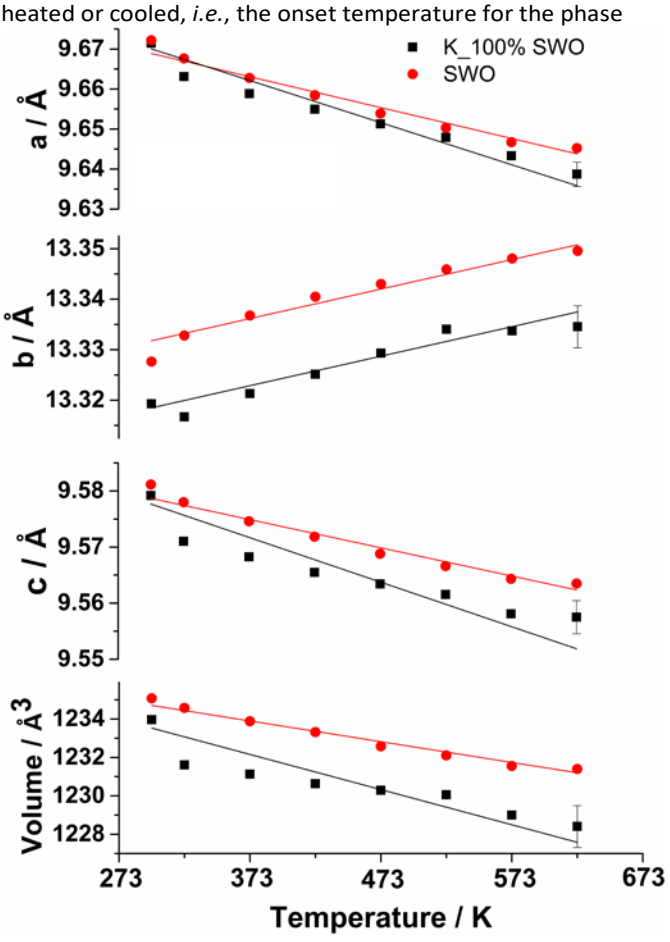

Figure 6 Evolution of the lattice parameters and cell volume for 0 and 100 % K discharged $Sc_2(WO_4)_3$ electrodes between 298 to 623 K.

Table 4: Refined crystallographic parameters of the K_2WO_4 phase identified at 973 K. The corresponding Rietveld refinement is shown in Figure 5(c). R_{wp} = 4.05 %, GOF = 3.02, space group *P*-3*m*1, *a* = 6.3620 (10) Å, *c* = 8.1884(4) Å, volume = 287.08(5) Å^3. Site occupancy factor (S.O.F); atomic displacement parameter (A.D.P). S.O.Fs were fixed throughout refinements.

Atom	*x*	*y*	*z*	S.O.F	A.D.P (Å^2)
K(1)	0.000	0.000	0.000	1	0.61(4)
K(2)	0.000	0.000	0.500	1	0.02
K(3)	0.3333	0.6667	0.8714(15)	1	0.29(1)
W	0.3333	0.6667	0.2949(15)	1	1.08(3)
O(1)	0.3333	0.6667	0.5294(15)	1	0.25(2)
O(2)	0.1611(4)	-0.1611(4)	0.2649(3)	1	0.24(2)

Table 5 Refined lattice parameters of K_2WO_4.

	a / Å	*c* / Å	v / Å^3
923 K	6.3903(9)	8.1939(5)	289.77(6)
1023 K	6.3122(8)	8.2343(8)	284.13(46)

change varies. The differences between the phase evolution observed by Warczewski[36] and that presented in this study may be attributed to the fact that the materials are mixed with PVDF and carbon black as part of the composite electrode and the electrochemical discharge process adds to the complexity of the structural problem.

Table 3 shows a comparison of the bond lengths calculated for the reported α-K_2SO_4 structure compared to the structural model of K_2WO_4, determined from Rietveld analysis of the 963 K data. The bond lengths of the refined K_2WO_4 structure are markedly different from the original α-K_2SO_4 phase. To the authors' knowledge, this is the first time the K_2WO_4 structure has been refined in the *P*-3*m*1 space group. It is interesting to note that there does not appear to be a crystalline Sc containing species present at higher temperatures. This suggests that either the additional minor peaks contain Sc or it is present as an amorphous or nano-crystalline component that is Sc-rich. Further, during cooling from 1023 K, the phase evolution is quite complicated, with a significant phase transition observed at 623 K. This may correspond to K_2WO_4 transforming to an orthorhombic *Ccmm* phase below 623 K. These could be a combination of Sc-containing phases crystallising or reactions with other components still present in the composite such as various forms of carbon.

Conclusions

The electrochemical performance of $Sc_2(WO_4)_3$ electrodes as an electrochemical host for potassium ions has been investigated using a combination of electrochemical, *ex situ* XRD and solid-state NMR studies. At the end of the 1st discharge, the $Sc_2(WO_4)_3$ structure is retained. ^{45}Sc and ^{39}K solid-state NMR of the K discharged electrode indicate the presence of a single highly symmetrical local environment for both Sc and K. *Ex situ* XRD studies indicated that low temperature thermal expansion mirrors that of the parent $Sc_2(WO_4)_3$, with minute changes observed up to 623 K. As the temperature is increased further for the 100 % K discharged $Sc_2(WO_4)_3$, there is the appearance of at least two phases, one of which has been identified as K_2WO_4, adopting a trigonal structure with space group *P*-3*m*1. Between 923 and 1023 K, this phase becomes the predominant phase and its structure has been refined for the first time. This phase was found to exhibit an exceptionally high NTE coefficient of α_{vol} = -1.90(10) x 10^{-4} K^{-1} between 923 and 1023 K. Upon cooling, the phase evolution observed is complex, with the appearance of numerous new reflections, some of which match the orthorhombic *Ccmm* phase of K_2WO_4, however full characterisation was not possible, based on the complexity of the XRD data obtained. The work presented here builds on the rich and complex phase evolution exhibited by $Sc_2(WO_4)_3$ electrodes upon discharge in electrochemical cells and subsequent thermal treatment. This work highlights the effectiveness of electrochemical activation for inducing interesting structural changes and/or the modification of physical properties in host materials.

Conflicts of interest

There are no conflicts to declare.

Acknowledgements

Junnan Liu would like to thank the support of the China Scholarship Council and UNSW for PhD funding. Damian Goonetilleke acknowledges the support of the Research Training Scheme. This work was financially supported by the Australian Research Council DECRA (DE160100237) and DP (DP170100269) programs. Part of this research was undertaken on the Powder Diffraction beamline at the Australian Synchrotron, part of the Australian Nuclear Science and Technology Organisation (ANSTO). Neeraj Sharma would like to thank the Royal Society of Chemistry for the travel funds to visit Durham University under the Researcher Mobility Scheme. Karen Johnston and Abby Haworth would like to thank David Apperley for experimental assistance and the EPSRC for an EPSRC Doctoral Training Partnership award (EP/N509462/1). Authors wish to acknowledge PhD student Jennifer H. Stansby for her assistance in collecting variable-temperature XRD data.

References

1. S. S. Han and W. A. Goddard, *The Journal of Physical Chemistry C*, 2007, **111**, 15185-15191.
2. N. Lock, Y. Wu, M. Christensen, L. J. Cameron, V. K. Peterson, A. J. Bridgeman, C. J. Kepert and B. B. Iversen, *The Journal of Physical Chemistry C*, 2010, **114**, 16181-16186.
3. Y. Wu, A. Kobayashi, G. J. Halder, V. K. Peterson, K. W. Chapman, N. Lock, P. D. Southon and C. J. Kepert, *Angew. Chem.*, 2008, **120**, 9061-9064.
4. X. Shen, C. Viney, E. R. Johnson, C. Wang and J. Q. Lu, *Nat Chem*, 2013, **5**, 1035-1041.
5. X. G. Zheng, H. Kubozono, H. Yamada, K. Kato, Y. Ishiwata and C. N. Xu, *Nat. Nanotechnol.*, 2008, **3**, 724-726.
6. K. Takenaka, *Frontiers in chemistry*, 2018, **6**, 267.
7. C. Lind, *Materials*, 2012, **5**, 1125-1154.
8. T. Mary, J. Evans, T. Vogt and A. Sleight, *Science*, 1996, **272**, 90-92.
9. C. Martinek and F. Hummel, *Journal of the American Ceramic Society*, 1968, **51**, 227-228.
10. J. Evans, T. Mary and A. Sleight, *Physica B: Condensed Matter*, 1997, **241**, 311-316.
11. P. Forster and A. Sleight, *Int. J. Inorg. Mater.*, 1999, **1**, 123-127.
12. A. Sleight, *Endeavour*, 1995, **19**, 64-68.
13. R. Mittal, S. L. Chaplot, H. Schober and T. A. Mary, *Neutron News*, 2002, **13**, 33-35.
14. J. Evans, T. Mary and A. Sleight, *J. Solid State Chem.*, 1998, **137**, 148-160.
15. B. L. Ellis, K. T. Lee and L. F. Nazar, *Chem. Mater.*, 2010, **22**, 691-714.
16. B. Schulz, H. L. Andersen, O. K. Al Bahri, B. Johannessen, J. Liu, S. Primig and N. Sharma, *CrystEngComm*, 2018, **20**, 1352-1360.
17. D. Goonetilleke, N. Sharma, J. Kimpton, J. Galipaud, B. Pecquenard and F. Le Cras, *Frontiers in Energy Research*, 2018, **6**, 64.
18. M. Kriener, K. Segawa, Z. Ren, S. Sasaki, S. Wada, S. Kuwabata and Y. Ando, *Physical Review B*, 2011, **84**, 054513.
19. H. L. Andersen, O. K. Al Bahri, S. Tsarev, B. Johannessen, B. Schulz, J. Liu, H. E. Brand, M. Christensen and N. Sharma, *Dalton Transactions*, 2018, **47**, 1251-1260.
20. J. Liu, H. L. Andersen, O. K. Al Bahri, S. Bhattacharyya, A. Rawal, H. E. Brand and N. Sharma, *Dalton Transactions*, 2018, **47**, 14604-14611.
21. S. Wang, D. Goonetilleke and N. Sharma, *Inorganic chemistry*, 2018, **57**, 10633-10639.
22. A. Goodwin and C. Coates, *Materials Horizons*, 2018, **6**.
23. D. R. Black, D. Windover, A. Henins, J. Filliben and J. P. Cline, *Powder Diffr.*, 2011, **26**, 155-158.
24. B. H. Toby and R. B. Von Dreele, *Journal of Applied Crystallography*, 2013, **46**, 544-549.
25. K. Momma and F. Izumi, *Journal of Applied Crystallography*, 2008, **41**, 653-658.
26. M. Hess, T. Sasaki, C. Villevieille and P. Novák, *Nature communications*, 2015, **6**, 8169.
27. J. Liu and N. Sharma, *Inorg. Chem.*, 2019, In press, 10.1021/acs.inorgchem.9b01116.
28. N. Kim, C.-H. Hsieh and J. F. Stebbins, *Chemistry of Materials*, 2006, **18**, 3855-3859.
29. K. J. MacKenzie and M. E. Smith, *Multinuclear solid-state nuclear magnetic resonance of inorganic materials*, Elsevier, 2002.
30. H. L. Andersen, O. K. Al Bahri, S. Tsarev, B. Johannessen, B. Schulz, J. Liu, H. E. Brand, M. Christensen and N. Sharma, *Dalton Transactions*, 2018.
31. A. Van Den Akker, A. Koster and G. Rieck, *Journal of Applied Crystallography*, 1970, **3**, 389-392.
32. N. Brese and M. O'keeffe, *Acta Crystallographica Section B*, 1991, **47**, 192-197.
33. M. Azuma, W.-t. Chen, H. Seki, M. Czapski, S. Olga, K. Oka, M. Mizumaki, T. Watanuki, N. Ishimatsu and N. Kawamura, *Nature communications*, 2011, **2**, 347.
34. K. Takenaka, Y. Okamoto, T. Shinoda, N. Katayama and Y. Sakai, *Nature communications*, 2017, **8**, 14102.
35. Y. Sun, C. Wang, Y. Wen, K. Zhu and J. Zhao, *Applied Physics Letters*, 2007, **91**, 231913.
36. J. Warczewski, *Phase Transitions: A Multinational Journal*, 1979, **1**, 131-142.
37. A. Koster, F. Kools and G. Rieck, *Acta Crystallographica Section B*, 1969, **25**, 1704-1708.
38. A. Guarnieri, A. Moreira, C. Pinheiro and N. Speziali, *Physica B: Condensed Matter*, 2003, **334**, 303-309.

Table of contents image and text

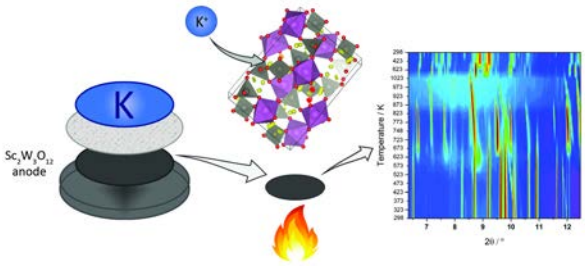

Electrochemical discharge followed by thermal treatment produces K_2WO_4 and other phases. K_2WO_4 features a large negative thermal expansion coefficient between 923-1023 K.